Chemistry Europe
European Chemical Societies Publishing

WILEY VCH

Excellence in Chemistry Research

Announcing our new flagship journal

- Gold Open Access
- Publishing charges waived
- Preprints welcome
- Edited by active scientists

Meet the Editors of *ChemistryEurope*

Luisa De Cola
Università degli Studi di Milano Statale, Italy

Ive Hermans
University of Wisconsin-Madison, USA

Ken Tanaka
Tokyo Institute of Technology, Japan

Chemistry–A European Journal
Research Article
doi.org/10.1002/chem.202203477
Chemistry Europe
European Chemical Societies Publishing
www.chemeurj.org

Special Collection

Modulation of Chiroptical and Photophysical Properties in Helicenic Rhenium(I) Systems: The Use of an *N*-(Aza[6]helicenyl)-NHC Ligand

Etienne S. Gauthier,[a] Laura Abella,[b] Elsa Caytan,[a] Thierry Roisnel,[a] Nicolas Vanthuyne,[c] Ludovic Favereau,[a] Monika Srebro-Hooper,[d] J. A. Gareth Williams,*[e] Jochen Autschbach,*[b] and Jeanne Crassous*[a]

Abstract: The photophysical and chiroptical properties of a novel, chiral helicene-NHC–Re(I) complex bearing an *N*-(aza[6]helicenyl)-benzimidazolylidene ligand are described, showing its ability to emit yellow circularly polarized luminescence. A comparative analysis of this new system with other helicene-Re(I) complexes reported to date illustrates the impact of structural modifications on the emissive and absorptive properties.

Introduction

N-Heterocyclic carbenes (NHCs) have impacted all fields related to coordination chemistry and organometallic chemistry,[1,2] following the first isolation of a crystalline and stable carbene by Arduengo et al. some three decades ago.[3] NHCs are strongly electron-donating species, able to form stable metal-carbon bonds, and they are compatible with a large variety of transition metal centers. These features have enabled applications in a wide range of domains including homogenous catalysis,[4–6] applicative materials functionalization,[7,8] and therapeutics.[9,10] Luminescent complexes comprising monodentate or bidentate NHC ligands have been investigated and even implemented in electroluminescent devices, owing to their high stability and efficient emission.[11–14] These properties are supported by the strong-field character of the NHC ligand and its influence on the metal orbitals and electronic transitions. Among the transition metal NHC systems, Re(I) tricarbonyl complexes $[ReX(CO)_3(:C^{\wedge}N)]$ have been reported[15,16] and their luminescence properties were analyzed in comparison to the well-established parent $[ReX(CO)_3(N^{\wedge}N)]$ systems.[17] In the above generic formulas, X is a halogen, $N^{\wedge}N$ is a bidentate ligand incorporating two N-coordinating units (e.g., bipyridines or diamines), while $:C^{\wedge}N$ is an equivalent system where an NHC carbon atom replaces one of the N-coordinating units.

Because of the versatility of NHC chemistry, it is possible to access a great number of molecular structures, including structures containing sources of chirality. It is therefore possible to obtain chiral complexes that are attractive as enantioselective catalysts[5,18] or as circularly polarized luminophores, for example.[19–21] Using the configurationally stable helical chirality provided by a helicene, an *ortho*-fused π-conjugated system,[22,23] diverse helically chiral complexes of Au(I),[21,24,25] Au(III),[21] Rh(I),[21] Ru(II),[26] Ni(II),[27] Ir(I),[24] Ir(III),[19,28–31] and Cu(I)[32] have been recently prepared and studied. Furthermore, the first chiral NHC–Re(I) complexes, **A-I** and **A-Cl**, were reported by us in 2020, using an *N*-(pyridyl)-[5]helicene-imidazolylidene as the $:C^{\wedge}N$ ligand (**A-X** in Figure 1).[33] Investigation of the photophysical and chiroptical properties revealed appealing features such as: i) intense electronic circular dichroism (ECD), ii) green circularly polarized luminescence (CPL) with dissymmetry factors, g_{lum}, up to $\pm 5\times10^{-3}$, and iii) long emission lifetimes up to 0.7 ms, which could be tuned by subtle structural modulations including the identity of the halide ligand and the stereochemical environment. The very first example of a

[a] Dr. E. S. Gauthier, Dr. E. Caytan, Dr. T. Roisnel, Dr. L. Favereau, Dr. J. Crassous
Univ Rennes, CNRS, ISCR – UMR 6226
35000 Rennes (France)
E-mail: jeanne.crassous@univ-rennes1.fr
[b] Dr. L. Abella, Prof. J. Autschbach
Department of Chemistry
University at Buffalo
State University of New York
14260 Buffalo, New York (USA)
E-mail: jochena@buffalo.edu
[c] Dr. N. Vanthuyne
Aix Marseille University
CNRS Centrale Marseille, iSm2
13284 Marseille (France)
[d] Dr. M. Srebro-Hooper
Faculty of Chemistry
Jagiellonian University
Gronostajowa 2, 30-387 Krakow (Poland)
[e] Prof. J. A. G. Williams
Department of Chemistry
Durham University
DH1 3LE Durham (UK)
E-mail: j.a.g.williams@durham.ac.uk

Supporting information for this article is available on the WWW under https://doi.org/10.1002/chem.202203477

This publication is part of a Special Collection on aromatic chemistry in collaboration with the "19th International Symposium on Novel Aromatic Compounds (ISNA-19)".

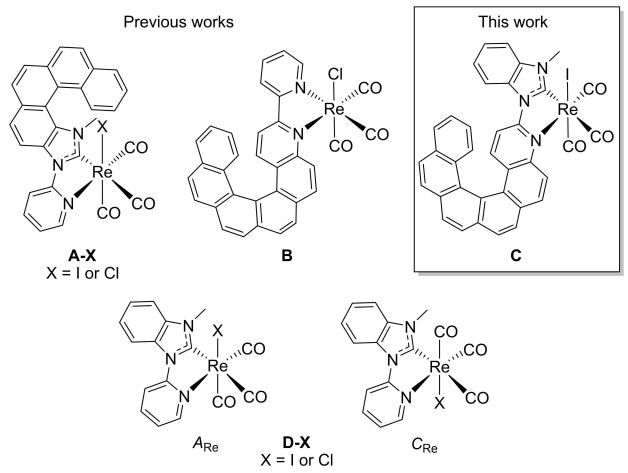

Figure 1. Examples of helicene-Re(I) complexes reported in the literature (**A** and **B**)[33,34] and the novel structure described in this work (**C**). Model non-helicenic systems **D** with the corresponding A_{Re}/C_{Re} stereodescriptors are also depicted.[33]

helicenic Re(I) complex bearing an *N*^*N*-coordinating [6]helicene-bipyridine ligand, **B** in Figure 1, was also prepared by us, in 2015, and found to display CPL in the red spectral region.[34] In this regard, it is appealing to investigate an analogue in which the *N*^*N* ligand is replaced by a :*C*^*N* ligand; i.e., with an NHC in place of the pendant pyridyl substituent of the azahelicene, as opposed to the NHC unit being incorporated within the helicene itself as it was in **A-X**. The resulting architecture can be thought of as transitioning between **A** and **B**. The impact of such structural and electronic modifications on the absorption and emission of polarized and unpolarized light could be of wide-ranging interest.

Accordingly, in this work, we report on the synthesis of a novel chiral Re(I) complex **C** with an *N*-(aza[6]helicenyl)-benzimidazolylidene ligand (see Figure 1). It possesses two stable stereogenic elements, viz. a [6]helicene and an octahedral rhenium(I) center. Enantiomerically and diastereomerically pure samples were obtained. Their photophysical (UV-Vis and luminescence) and chiroptical (ECD, optical rotation – OR, and CPL) properties were studied. Comparative analyses of this system with helicene-Re(I) complexes **A** (having a π-helical, more conjugated and less donating carbene) and **B** (with a less donating 2-pyridyl unit rather than a carbene), and also with parent (non-helicenic) complexes **D**[33] were performed to delineate the structure-property relationships in these types of compounds.

Synthesis and structural characterizations

The synthesis of novel Re(I) complexes and of their proligand precursors is depicted in Scheme 1. An Ullmann-type coupling was performed between benzimidazole and enantiopure (*P*)- or (*M*)-3-bromo-4-aza[6]helicene **1**, whose preparation was previously reported by our group.[35] Using CuI/L-proline as the catalytic system,[36] the coupling product (*P*)-**2** was successfully obtained from (*P*)-**1** in 67% yield; (*M*)-**2** was similarly obtained from (*M*)-**1** with a yield of 63%. Due to the prolonged reaction times at reasonably high temperature (at least 63 h at 110 °C), chiral HPLC analyses were conducted to verify the optical purity of the obtained coupling product (see the Supporting Information). Analytical measurements with the Chiralpak IF column revealed that both (*M*)-**2** and (*P*)-**2** have *ee* values >98%, indicating that the chirality is preserved thanks to the high configurational stability of the [6]helicene.[22,37] Next, methylation with MeI in acetonitrile at 110 °C gave the imidazolium iodide salt (*P*)-**3** in 90% yield; (*M*)-**3** was similarly obtained in 99% yield. Compounds **2** and **3** were fully characterized by ^{1}H and ^{13}C NMR spectroscopy and mass spectrometry (see Supporting Information). Additionally, single crystals of (*P*)-**3** were obtained by slow diffusion of pentane vapors into a dichloro-

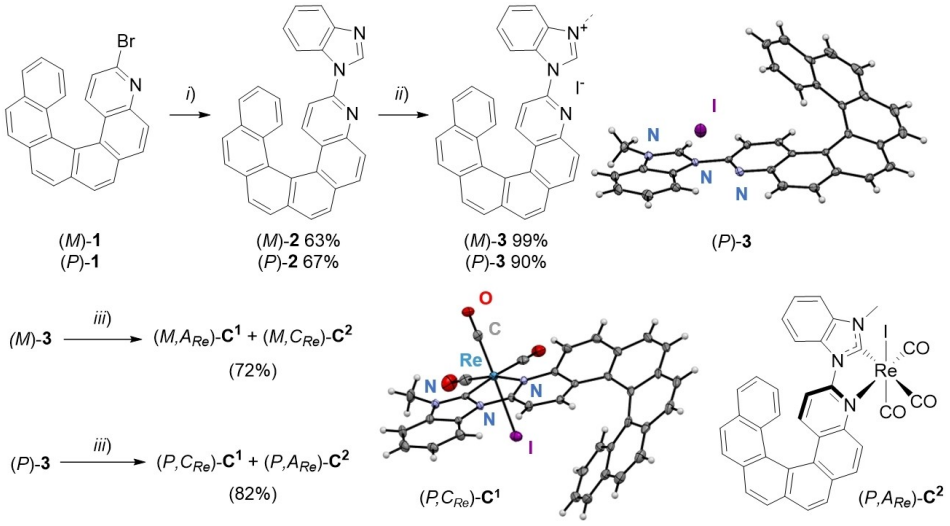

Scheme 1. Synthetic route to the stereoisomers of complex **C**. *i*) benzimidazole, K_2CO_3, CuI (cat.), L-Pro (cat.), DMSO, 110 °C, 65 h; *ii*) MeI, MeCN, reflux, overnight; *iii*) $ReCl(CO)_5$, K_2CO_3, toluene, reflux, 22 h. X-ray structures of (*P*)-**3** and (*P*,C_{Re})-**C**[1].

methane solution and were analyzed by X-ray diffraction. The benzimidazolium iodide salt crystallized in the non-centrosymmetric $P2_1$ space group, confirming the enantiopure nature of the crystal which displays only (*P*) helices in the unit cell, with a helicity angle (defined as the dihedral angle between terminal rings) of 50.09°, a classical value for [6]helicenes;[34,38] see Scheme 1. In the crystal, the aza[6]helicenyl-benzimidazolium molecules are oriented in a zig-zag fashion, with the iodide anions occupying the inner space between them. Intermolecular π-π contacts can be noted between imidazolium rings and [6]helicene terminal rings of the contiguous molecules (distance between two centroids = 3.548 Å, see Supporting Information), thus leading to homochiral supramolecular columns along the *b* axis.

Enantiopure imidazolium iodide salts (*P*)- and (*M*)-**3** were then used to prepare the target complexes (*P*)-**C**^{1,2} and (*M*)-**C**^{1,2} as a mixture of epimers due to the presence of the two stereogenic elements (the configurationally stable aza[6]helicene and the octahedral Re(I) center).[39,40] Reaction of the enantiopure salt with $ReCl(CO)_5$ as the Re source and K_2CO_3 in refluxing toluene[15] afforded (*P*)-**C**^{1,2} and (*M*)-**C**^{1,2}, respectively, in 82% and 72% yield. ^{1}H NMR spectra of the crude mixture confirmed the absence of the starting benzimidazolium precursor (lack of signal around 10–11 ppm for the pre-carbenic proton) and the effective formation of the Re(I) complexes (appearance of two sets of signals corresponding to two diastereoisomers with ratios of 54:46 for (*P*)-**C**^{1,2} and 71:29 for (*M*)-**C**^{1,2}, see Supporting Information). The presence of split signals in unequal ratio suggests that diastereoselectivity arises during the metalation of the helically chiral ligand, with formation of a major and a minor diastereoisomer. However, after work-up and silica gel chromatography, the diastereomeric ratio evolved to around 1:1 suggesting high sensitivity of the metal environment to the reaction and purification conditions (temperature, solubility, light). Nevertheless, the purified neutral complexes appeared to be configurationally stable in the dark. The diastereomeric pairs could be further separated using semi-preparative chiral HPLC (see below).

Diastereomerically and enantiomerically pure samples of complex **C** were thus obtained with *de* and *ee* values > 98% (see Supporting Information for details). Full structural characterizations of the enantiomers were conducted (see Supporting Information). A complete analysis of the diastereomeric complexes was performed by NMR spectroscopy, and X-ray crystallography analysis was also carried out on suitable single crystals of the (*P*)-**C**^{1} diastereoisomer grown by slow diffusion of pentane vapors into a dichloromethane solution. The compound crystallized in the $P2_12_12_1$ non-centrosymmetric space group showing the (P,C_{Re})-**C**^{1} enantiomer, which enabled the assignment of the relative configuration for all stereoisomers (see Scheme 1 and Supporting Information). The rhenium(I) center is coordinated in the expected pseudo-octahedral geometry by the bidentate (*P*)-aza[6]helicenyl-benzimidazolylidene ligand, with the three carbonyl ligands in a mutually *fac* arrangement, and the iodide ligand in apical position defining a (C_{Re}) configuration (see Supporting Information for the assignment of A_{Re}/C_{Re} stereodescriptors).[39,40] The NHC ring is almost coplanar with the N-coordinating ring: the N_{aza}–C_{aza}–$N_{carbene}$–$C_{carbene}$ dihedral angle is only 1.39°. The bond lengths Re–N_{aza} (2.245 Å), Re–$C_{carbene}$ (2.111 Å) and Re–I (2.814 Å) are within the range of those already reported for [ReX(CO)$_3$(:$C^\wedge N$)] complexes including helicenic ones,[15,33,34] and indicate the efficient electronic interaction between the bidentate NHC-aza[6]helicene ligand and the metal. This was further confirmed by the results of charge and bonding-energy decomposition analysis[41,42] demonstrating :$C^\wedge N$→Re σ-donation (dominant) and Re→:$C^\wedge N$ π-back-donation underpinning the NHC-aza[6]helicene-Re(I) interactions. Note that a description of computational protocols used in this work is provided in the Supporting Information, with a full set of calculated results and their analysis. Finally, the helicity angle of 44.77° shown by the aza[6]helicenyl-benzimidazolylidene ligand falls within the same range as other [6]helicene derivatives.[34,38]

Photophysical characterization: absorption and emission

The UV-Vis absorption spectra of the benzimidazole precursor **2** and the two diastereoisomers of **C**, i.e. (M,A_{Re})-**C**^{1} and (M,C_{Re})-**C**^{2}, were recorded in CH_2Cl_2 at concentrations around 10^{-5} M (Figure 2a). One can notice similar spectral features between the benzimidazole intermediate **2** and the complexes **C**^{1,2}, which indicate the expected major contribution of the helicenic unit to the excitations observed in the complexes. Overall, all

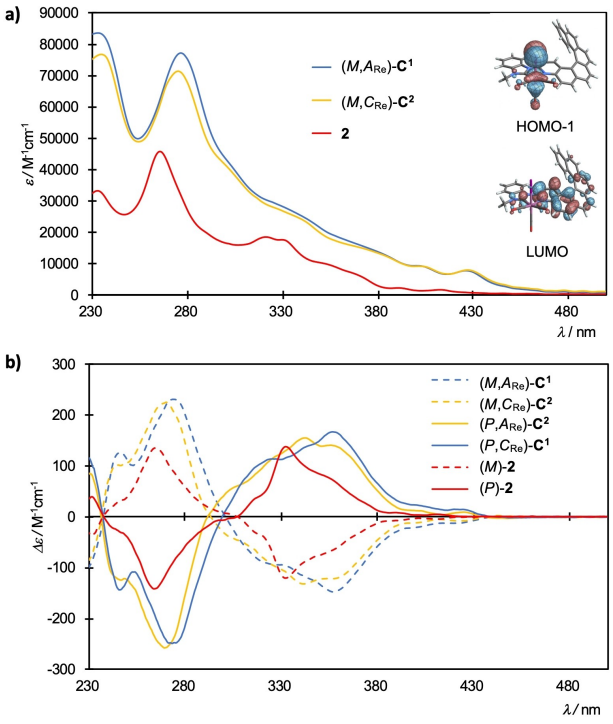

Figure 2. a) UV-Vis absorption and b) ECD spectra of enantiopure benzimidazole **2** and complexes **C**^{1} and **C**^{2} measured in CH_2Cl_2 at 10^{-5} mol L^{-1}. Relevant MOs for **C**^{1} from the ground-state calculation are also presented (isosurfaces: ±0.03 au). See Supporting Information for computational details and a full set of calculated data.

bands appear more intense and slightly red-shifted for $\mathbf{C}^{1,2}$ as compared to **2** which likely results from the stronger conjugation in $\mathbf{C}^{1,2}$ due to the presence of the metal coordination. Both $\mathbf{C}^1$ and $\mathbf{C}^2$ show essentially the same spectra except that the former has slightly higher absorptivity at shorter wavelengths.

The UV-Vis spectrum of **2** displays two bands of high intensity at 234 nm ($\varepsilon \sim 32500\ M^{-1}cm^{-1}$) and at 265 nm ($\varepsilon \sim 45700\ M^{-1}cm^{-1}$) followed by two signals around 320 nm ($\varepsilon \sim 18400\ M^{-1}cm^{-1}$) and 331 nm ($\varepsilon \sim 17500\ M^{-1}cm^{-1}$). At lower energies, a shoulder is present around 360 nm ($\varepsilon \sim 8200\ M^{-1}cm^{-1}$) along with two bands at 392 and 413 nm ($\varepsilon \sim 1600\ M^{-1}cm^{-1}$). Regarding the complexes, time-dependent density functional theory (TD-DFT) calculations gave very good agreement with the experimental spectra (see Supporting Information) and demonstrated that the observed absorption bands are composed of mixtures of charge-transfer (CT) transitions involving the metal (M), the halide ligand (X) and the NHC-azahelicenic π-system (L). Specifically, bands of higher energies and higher intensities at 233 nm ($\varepsilon \sim 80000\ M^{-1}cm^{-1}$) are assigned to admixed MLCT, ILCT and π-π* transitions within L. The band at 275 nm ($\varepsilon \sim 75000\ M^{-1}cm^{-1}$) and the shoulder around 300 nm ($\varepsilon \sim 41000\ M^{-1}cm^{-1}$) are attributed to admixed MLCT, XLCT and ILCT transitions. Two additional shoulders are present in both measurement and calculations. The one around 330 nm ($\varepsilon \sim 26000\ M^{-1}cm^{-1}$) is attributed to ILCT transitions and the one around 380 nm ($\varepsilon \sim 13000\ M^{-1}cm^{-1}$) results from combined MLCT, XLCT and ILCT transitions. Finally, the bands corresponding to the lowest energies are located at 403 nm ($\varepsilon \sim 9000\ M^{-1}cm^{-1}$) and 428 nm ($\varepsilon \sim 7800\ M^{-1}cm^{-1}$) and assigned to transition between the HOMO-1, localized on the OC–Re–I moiety, and the LUMO which is centered mainly on the NHC-pyridyl and delocalized over the adjacent rings of the helicene, giving mixed MLCT and XLCT character to the observed excitation [see molecular orbitals (MOs) in Figure 2a and Supporting Information].

The helicene derivative **2** displays vibrationally structured blue fluorescence in CH_2Cl_2 solution at room temperature, $\lambda^{0,0} =$ 421 nm (see Supporting Information, Figure S1.24 and Table 1). The fluorescence quantum yield under these conditions is 7% and the emission decays mono-exponentially with a lifetime of 7 ns. In a frozen glass at 77 K, the highly structured fluorescence is slightly blue-shifted and, under these conditions, is accompanied by vibrationally structured phosphorescence in the region 500–700 nm ($\lambda^{0,0} = 520$ nm; Figure S1.24 and Table 1). The fluorescence and phosphorescence lifetimes at 77 K are 12 ns and 1.8 s, respectively. Overall, the emission behavior of **2** is quite typical of rigid, highly conjugated carbocycles, N-heterocycles, and helicene-based ligands previously studied.

Complexes $\mathbf{C}^1$ and $\mathbf{C}^2$ were found to be yellow phosphorescent emitters in deoxygenated CH_2Cl_2 solution at room temperature, displaying broad emission spectra with λ_{max} around 557 nm (Figure 3a). The emission is strongly quenched by dissolved molecular oxygen, consistent with its assignment as phosphorescence. The triplet state origin of the emission was further supported by measurements of long emission lifetime values in deoxygenated conditions: $\tau = 23$ μs for (M,C_{Re})-$\mathbf{C}^2$ and $\tau = 18$ μs for (M,A_{Re})-$\mathbf{C}^1$. The values are around 20-fold shorter in air-equilibrated solutions (Table 1). We note that (M,C_{Re})-$\mathbf{C}^2$ emits with a slightly higher efficiency than its epimer (M,A_{Re})-$\mathbf{C}^1$: the phosphorescence quantum yields Φ are, respectively, 13% and 9%. This difference between the epimers apparently stems largely from higher non-radiative decay constants Σk_{nr} for (M,A_{Re})-$\mathbf{C}^1$ than for (M,C_{Re})-$\mathbf{C}^2$, as the radiative decay constants k_r are more similar (Table 1). In comparison with the complexes

Table 1. UV-Visible, emission data and CPL values for the proligand **2** and helicene-NHC-rhenium complexes $\mathbf{C}^{1,2}$ studied in this work and selected data for the systems **A**, **B** and **D** (in CH_2Cl_2 at 295 K or in EPA at 77 K).

System		Absorption λ_{max} [nm] (ε [$M^{-1}cm^{-1}$])[a]	Emission λ_{max} [nm][b]	$\Phi \times 10^{-2}$[c]	τ[d]	k_r [s^{-1}][e]	Σk_{nr} [s^{-1}][e]	g_{lum}	Emission at 77 K[f]	
									λ_{max} [nm]	τ_{phos}
2	(*M*)	234 (29500), 267 (44700), 325 (17600), 332 (17040), 355sh (9510), 394 (1640), 415 (1160)	419, 442, 468, 506	7.0	7 ns	1.1×10^7	1.4×10^8	-2.5×10^{-3}	413, 437, 465 (F) 520, 567, 614, 666 (P)	12 ns (F) 1.8 s (P)
A-I[33]	(M,A_{Re})	291 (48667), 310sh (42561), 380 (6783), 397 (6093), 426sh (1783)	520, 556	0.81	50 μs	160	20000	$+4.4\times10^{-4}$	510, 551, 595, 654sh	7700 μs
B[34]	(M,C_{Re})	–	673	0.16	33 ns	–	–	-2.8×10^{-3}	554, 601, 654sh	43 μs
C	(M,A_{Re})	235 (83200), 279 (76000), 334sh (27000), 404 (9090), 430 (7240)	556sh, 593	8.7	18 μs [0.96 μs]	4800	51000	-1.1×10^{-3}	534, 575, 623	670 μs
	(M,C_{Re})	235 (76700), 277 (70700), 332 (26200), 405 (8970), 430 (7620)	558sh, 596	13	23 μs [1.1 μs]	5600	38000	$+1.9\times10^{-3}$	537, 581, 630, 704	400 μs[g]
D-I[33]	*rac*	285 (17400), 370 (4070), 415 (1270)	511	0.13	110 ns	12000	9.0×10^6	~0	458	5.2 μs

[a] In CH_2Cl_2 at 295 K. [b] In deoxygenated CH_2Cl_2 at 295 K; $\lambda_{max} = \lambda^{0,0}$ in each case. [c] Quantum yields in deoxygenated CH_2Cl_2 at 295 K: for **2**, measured with quinine sulfate in 1 M H_2SO_4(aq.) as the standard ($\Phi = 0.55$); for complexes **C**, measured using $[Ru(bpy)_3]Cl_2$ (aq.) as the standard, for which $\Phi = 0.04$.[43] [d] Luminescence lifetimes in deoxygenated CH_2Cl_2 at 295 K, estimated uncertainty in the values is around ±10%; the values in parentheses refer to measurements on the corresponding air-equilibrated solutions. [e] Radiative k_r and non-radative Σk_{nr} decay constants estimated assuming that the emissive triplet state is formed with unit efficiency such that $k_r = \Phi/\tau$ and $\Sigma k_{nr} = (1-\Phi)/\tau$. [f] In EPA = diethyl ether/isopentane/ethanol, 2:2:1, v/v. [g] The fit to mono-exponential decay is rather poor in this instance; a bi-exponential fit gives two components of 700 and 280 μs (43:57 weighting).

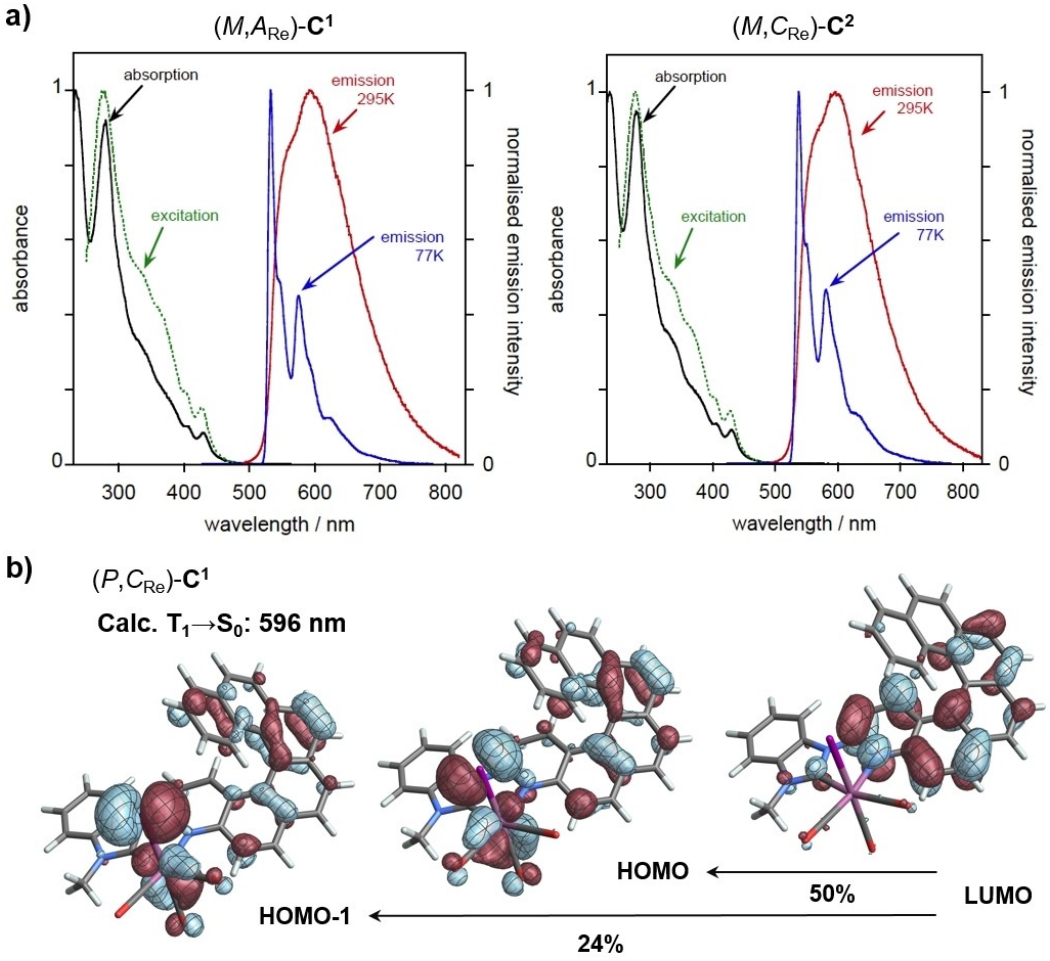

Figure 3. a) Absorption (black lines), excitation (λ_{em} = 585 nm, dashed green lines), and emission (λ_{ex} = 430 nm, red lines) spectra for (M,A_{Re})-**C¹** (left) and (M,C_{Re})-**C²** (right), in CH_2Cl_2 at 295 ± 1 K, together with their respective emission spectra at 77 K in EPA (λ_{ex} = 400 nm, blue lines). b) Computed $T_1 \rightarrow S_0$ phosphorescence vertical transition wavelength along with the corresponding MO-pair contributions (isosurfaces: ± 0.03 au at the T_1 equilibrium structure) for **C¹**. Note that at the S_0 equilibrium structure, HOMO to HOMO-2 are near-degenerate (Supporting Information, Figure S2.3). Going to the T_1 equilibrium structure, there is some reorganization among these MOs, which is the reason why HOMO-1 appears different here than in Figure 2.

bearing a [5]helicene-imidazolylidene ligand,[33] **A-I** and **A-Cl** (Figure 1; **A-I**: λ_{max} = 520 nm), the red-shift in emission can be rationalized by the slight extension of the π-electron conjugation in **C**, which comprises a [6]helicene fragment as opposed to the [5]helicenic unit in **A-I** and **A-Cl**. Interestingly, the emission profiles at room temperature show only a hint of vibrational structure, contrary to **A-I** and **A-Cl** where it is better resolved, which possibly suggests less prominent involvement of the π-conjugated part of the chromophore and a more pronounced MLCT character to the radiative transitions.[33]

On the other hand, the emission of complexes **C** is blue-shifted compared to **B** (λ_{max} = 673 nm). Recall that complex **B** has a bidentate bipyridyl $N^{\wedge}N$-coordinating unit instead of $:C^{\wedge}N$ (Figure 1). The large difference in the emission maximum is attributed to the different electronic behaviors of the N-heterocyclic carbene ligand compared to the pyridyl ring.[34] The NHC is a strong-field ligand which induces stronger destabilization of the LUMO compared to the pyridyl unit, resulting in an increase in the HOMO-LUMO gap and thus a blue-shift in the emission. A further striking difference is the much higher emission efficiency and longer lifetime of the new complexes **C** compared to **B** (see Table 1), the low energy of the latter's excited state favoring efficient non-radiative decay pathways. Finally, compared to parent model **D**, isomeric complexes **C**^{1,2} not only exhibit longer lifetimes and red-shifted emission but also larger quantum yields, thus highlighting the considerable added value of such helical architectures.

TD-DFT calculations conducted at the T_1 excited-state equilibrium structure are in accordance with the experimental results of the luminescence for **C** (see Supporting Information). The computed data were compared with those obtained for **A-I**, **A-Cl**, **B** and **D** to identify the origin of the differences in emission energy and other photophysical properties in this series of Re(I) complexes.[33,34] The conclusions of this analysis support the experimental findings presented above. In particular, the calculations revealed that, despite having the same type of T_1 excited state (involving the π-electron system of the helicenic ligand L together with the metal M and halide ligand

X orbitals via a mixed MLCT/XLCT/ILCT character; see Figure 3b and Supporting Information), the MLCT contribution in comparison with the XLCT/ILCT varies in **A**, **B** and **C** depending on the structure of the helicenic ligand. It appears that the MLCT character increases when going from a [5]helicenic-NHC ligand (**A-I** and **A-Cl**) to an aza[6]helicenic-NHC ligand (**C**) (as also concluded from the experimental data above) and then to [6]helicenic-bipyridine (**B**). For the model system **D** that lacks the helicene unit, the phosphorescence transition corresponds predominantly to MLCT.[33] The change in MLCT character explains the reduction of the emission lifetimes: with the stronger participation of the metal, the formally forbidden $T_1 \rightarrow S_0$ process is facilitated to a greater extent, leading to faster radiative decay and shorter observed lifetimes (see Table 1). Delocalization of the T_1 excited state across the helicenic ligand in **A**, **B** and **C** also explains the trend in their emission wavelengths, with substantial red-shifts compared to that for the non-helicenic **D** complex, as well as the qualitative trends in the resolution of vibrational structure.

In a frozen glass at 77 K, the emission spectra of **C** display a well-resolved vibrational progression of around 1340 cm^{-1} (typical of aromatic C=C stretching vibrations) and the luminescence lifetimes are greatly lengthened to $\geq$400 μs (Table 1). These changes may be attributed to a shift of the $T_1 \rightarrow S_0$ character to predominantly helicene-centered. With the rigidification of the system, CT states are typically destabilized more than ligand-centered (LC) states, owing to the greater degree of charge reorganization accompanying the formation of the former. It is possible that, at 77 K, the MLCT state is destabilized to lie above the helicene-centered state.[44] Similar observations were made also for complex **B**, which corroborates the idea of a stronger involvement of the metal center in the phosphorescence at room temperature (stronger MLCT character of the emission).[34]

Chiroptical properties

We also investigated the chiroptical properties (OR, ECD, and CPL) of both diastereoisomers of **C** and of their benzimidazole enantiopure precursors **2** and **3**. High molar optical rotations (MRs) were measured for the helicenic intermediates and Re(I) systems ($\pm$1.1–1.5×10^4 deg cm^2 $dmol^{-1}$, details are provided in the Supporting Information), as expected for [6]helicene derivatives. It should be noted that the fully organic helicenes **2** and **3** have MRs close to those of the complexes with two stereogenic elements (the helically chiral unit and the chirality-at-rhenium). The values for two epimers are only slightly different; for example, (P,C_{Re})-**C**^{1} and (P,A_{Re})-**C**^{2} display specific rotations of +1850 and +1660 deg cm^3 g^{-1} dm^{-1}, respectively.

The small difference in the ORs was corroborated by measurements of ECD in CH_2Cl_2 (Figure 2b). Enantiomeric pairs of **2** and **C** display, as they must, mirror-image optical activity within the measurement errors. The intermediate **2** displays the characteristic spectrum of an aza[6]helicenic system, very similar to the spectrum of **1** measured by us previously.[35] As shown in Figure 2b, the ECD for (*M*)-**2** exhibits a positive band at 265 nm ($\Delta\varepsilon$ = +134 M^{-1} cm^{-1}) and a negative band at 332 nm ($\Delta\varepsilon$ = −121 M^{-1} cm^{-1}); minor vibronic features can be observed. Regarding the rhenium complexes, the respective spectra of the two epimers are only slightly different. For example, (M,A_{Re})-**C**^{1} exhibits positive ECD bands at 245 nm ($\Delta\varepsilon$ = +124 M^{-1} cm^{-1}) and 275 nm (+230 M^{-1} cm^{-1}), then negative bands at 323 nm (−92 M^{-1} cm^{-1}), 356 nm (−148 M^{-1} cm^{-1}), 401 nm (−21 M^{-1} cm^{-1}) and 423 nm (−9 M^{-1} cm^{-1}). The ECD bands of (M,C_{Re})-**C**^{2} are a little less intense, notably at 244 nm ($\Delta\varepsilon$ = +102 M^{-1} cm^{-1}) and 270 nm (+225 M^{-1} cm^{-1}) and, slightly, at 401 nm (−12 M^{-1} cm^{-1}) and 424 nm (−8 M^{-1} cm^{-1}). Between 290 and 365 nm, the substructure of the ECD spectrum is different for (M,C_{Re})-**C**^{2}, with the appearance of extra bands at 302 nm ($\Delta\varepsilon$ = −38 M^{-1} cm^{-1}), 320 nm (−80 M^{-1} cm^{-1}), 340 nm (−131 M^{-1} cm^{-1}) and 360 nm (−120 M^{-1} cm^{-1}). Noteworthy, additional very weak bands (negative for *P* and positive for *M* helices) seem to be also present around 450 nm (see onset in Figure S1.21). Overall, very similar ECD signatures obtained for **C**^{1} and **C**^{2} highlight the small contribution of the Re unit and the stronger effect of the [6]helicene part on the dominant optically active electronic transitions. This was further corroborated by theoretical calculations (see below). Finally, it should be noted that, being [6]helicene derivatives, complexes **C**^{1,2} display ECD and OR magnitudes that are higher than [5]helicene-based **A-X** and closer to those of **B**, while – as expected – non-helicenic complex **D** displays much less intense chiroptical responses.[33,34]

Calculated ECD spectra of **C**^{1,2} obtained by TD-DFT[45,46] nicely agree with the experiments, showing the correct alternation of signs and correct absolute and relative bands intensities (see Supporting Information). A notable exception is the vibronic fine structure observed experimentally, which was not modelled in the calculations. For two diastereoisomers (e.g., (P,C_{Re})-**C**^{1} and (P,A_{Re})-**C**^{2}), the strong ECD band between 300 and 450 nm is attributed to mixed MLCT, XLCT and ILCT (excitation #5), whereas the one of opposite sign between 230 and 300 nm is assigned to a mix of MLCT, XLCT, ILCT and π-π* transitions within the helicenic ligand (see Supporting Information regarding the MOs involved in selected transitions). It appears that the nature of the strongly ECD-active excitations for both epimers is nearly identical, with no predominance of any kind of charge transfer for one diastereoisomer or the other. This appears different from the previously described system **A** possessing a smaller [5]helicene-NHC ligand[33] and which displayed some substantial ECD tuning upon changing the (C_{Re})/(A_{Re}) configuration.

Finally, CPL (fluorescence for **2** and phosphorescence for **C**) spectra were recorded in CH_2Cl_2 (Figure 4 and Supporting Information). The organic helicene **2** displays unambiguous CPL with two emission maxima at 425 and 447 nm and g_{lum} values at 425 nm of +3.0×10^{-3} for (*P*)-**2** and −2.5×10^{-3} for (*M*)-**2** (see Supporting Information). The CPL spectra for the rhenium(I) complexes were noisier (Figure 4). It is interesting to note that the CPL sign seems to be controlled by the configuration of the metal center: (P,A_{Re})-**C**^{2} and (M,A_{Re})-**C**^{1} display the negative CPL signal whereas (P,C_{Re})-**C**^{1} and (M,C_{Re})-**C**^{2} the positive one. This is compatible with the conclusions drawn from the analysis of the

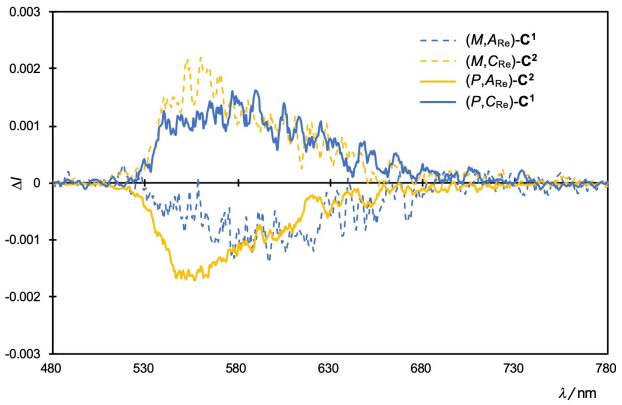

Figure 4. CPL spectra of enantiomers of $\mathbf{C}^{1,2}$ measured at 298 K in degassed CH_2Cl_2 (λ_{ex} = 400 nm).

unpolarized luminescence, viz. a strong involvement of the metal center (and its chirality) in the emissive properties. Similar findings, i.e., control of the CPL sign by the metal stereochemistry, were demonstrated for complexes **A-X**.[33,34] Furthermore, similar g_{lum} values were obtained for [6]helicenic complexes **B** and **C**, while the one for [5]helicene derivative **A-I** was found one order of magnitude lower (see Table 1). Overall, there is a slight difference in the g_{lum} values at 563 nm for (P,C_{Re})-$\mathbf{C}^1$ ($+1.1\times10^{-3}$) and for (M,C_{Re})-$\mathbf{C}^2$ ($+1.9\times10^{-3}$). Owing to the modest signal-to-noise ratio of the CPL spectra, the experimental uncertainty on g_{lum} is comparatively high, and the difference between the quoted values at 563 nm is accordingly not significant. The emission maxima of the total luminescence measured by the CPL spectrometer is shifted when going from (P,C_{Re})-$\mathbf{C}^1$ ($\lambda_{em,max,CPL}$ = 560 nm) to (M,C_{Re})-$\mathbf{C}^2$ ($\lambda_{em,max,CPL}$ = 568 nm). Considering the λ_{max} measured in the unpolarized emission (around 557 nm, see Table 1) and the broad profile of the room temperature luminescence, a wavelength of 563 nm can be chosen for the comparison of both g_{lum} factors as the total luminescence is high at this wavelength for both complexes.

Conclusion

A second series of optically active chiral rhenium(I) complexes possessing an *N*-(aza[6]helicenyl)-NHC ligand was prepared and characterized. The systems display yellow circularly polarized phosphorescence with emission lifetimes of several microseconds. The incorporation of the aza[6]helicenic moiety grafted onto the N-atom of NHC unit results in a change of the emissive properties in comparison with the first series of helically chiral [5]helicene-NHC-rhenium complexes described previously: a red-shift of the emission wavelength, a strong increase of the emission quantum yields and a reduction in the emission lifetimes,[33] which were attributed to a slight extension of the π-electron conjugation within the helicene moiety and the increase in the MLCT character of the T_1 excited state, respectively. As a direct consequence of using an aza[6]helicenic coordinating unit, very small differences are observed in the chiroptical properties between the different diastereoisomers. We have also been able to compare the properties of the complex with previously reported Re(I)-based red phosphors bearing an *N*^*N*-coordinating helical ligand.[34] It is found that the presence of the strong-field NHC ligand leads to a hypsochromic shift of the emission wavelength and a substantial enhancement of the photoluminescence quantum yield and lifetime. The new structure reported here represents, therefore, a hybrid system in between the two other reported examples and modulations of the properties were accordingly achieved. It reinforces the growing interests towards NHC–Re(I) complexes due to the ease with which diverse properties can be obtained. Going forward, we envisage further modifications of the coordination sphere (e.g., change of ligands, preparation of cationic complexes) to explore promising applications for bio-imaging or asymmetric photoredox catalysis.[47,48]

Acknowledgements

We thank the Centre National de la Recherche Scientifique (CNRS) and the University of Rennes. This work was supported by the Agence Nationale de la Recherche (ANR-16-CE07-0019 "Hel-NHC" grant). J. A. acknowledges the Center for Computational Research (CCR) for computational resources, and grant CHE-2152633 from the National Science Foundation for financial support. M. S.-H. thanks the PL-Grid Infrastructure and the ACC Cyfronet AGH in Krakow, Poland for providing computational resources. Part of this work has been performed using the PRISM core facility (Biogenouest©, Univ Rennes, Univ Angers, INRAE, CNRS, France).

Conflict of Interest

The authors declare no conflict of interest.

Data Availability Statement

The data that support the findings of this study are available in the supplementary material of this article.

Keywords: circularly polarized emission · density functional calculations · helicene · long-lived phosphorescence · N-heterocyclic carbene · rhenium(I)

[1] P. Bellotti, M. Koy, M. N. Hopkinson, F. Glorius, *Nat. Chem. Rev.* **2021**, *5*, 711–725.
[2] M. N. Hopkinson, C. Richter, M. Schedler, F. Glorius, *Nature* **2014**, *510*, 485–496.
[3] A. J. Arduengo, R. L. Harlow, M. Kline, *J. Am. Chem. Soc.* **1991**, *113*, 361–363.
[4] a) Y. Hong, L. Jarrige, K. Harms, E. Meggers, *J. Am. Chem. Soc.* **2019**, *141*, 4569–4572; b) J. Liu, X.-N. Xing, J.-H. Huang, L.-Q. Lu, W.-J. Xiao, *Chem. Sci.* **2020**, *11*, 10605–10613.
[5] D. Janssen-Müller, C. Schlepphorst, F. Glorius, *Chem. Soc. Rev.* **2017**, *46*, 4845–4854.

[6] S. Díez-González, N. Marion, S. P. Nolan, *Chem. Rev.* **2009**, *109*, 3612–3676.
[7] L. Mercs, M. Albrecht, *Chem. Soc. Rev.* **2010**, *39*, 1903–1912.
[8] C. A. Smith, M. R. Narouz, P. A. Lummis, I. Singh, A. Nazemi, C.-H. Li, C. M. Crudden, *Chem. Rev.* **2019**, *119*, 4986–5056.
[9] M.-L. Teyssot, A.-S. Jarrousse, M. Manin, A. Chevry, S. Roche, F. Norre, C. Beaudoin, L. Morel, D. Boyer, R. Mahiou, A. Gautier, *Dalton Trans.* **2009**, 6894–6902.
[10] K. M. Hindi, M. J. Panzner, C. A. Tessier, C. L. Cannon, W. J. Youngs, *Chem. Rev.* **2009**, *109*, 3859–3884.
[11] R. Visbal, M. C. Gimeno, *Chem. Soc. Rev.* **2014**, *43*, 3551–3574.
[12] R. Hamze, M. Idris, D. S. Muthiah Ravinson, M. C. Jung, R. Haiges, P. I. Djurovich, M. E. Thompson, *Front. Chem.* **2020**, *8*, 401.
[13] T.-Y. Li, X. Liang, L. Zhou, C. Wu, S. Zhang, X. Liu, G.-Z. Lu, L.-S. Xue, Y.-X. Zheng, J.-L. Zuo, *Inorg. Chem.* **2015**, *54*, 161–173.
[14] J. Lee, H.-F. Chen, T. Batagoda, C. Coburn, P. I. Djurovich, M. E. Thompson, S. R. Forrest, *Nat. Mater.* **2016**, *15*, 92–98.
[15] L. A. Casson, S. Muzzioli, P. Raiteri, B. W. Skelton, S. Stagni, M. Massi, D. H. Brown, *Dalton Trans.* **2011**, *40*, 11960–11967.
[16] P. V. Simpson, M. Falasca, M. Massi, *Chem. Commun.* **2018**, *54*, 12429–12438.
[17] M. Wrighton, D. L. Morse, *J. Am. Chem. Soc.* **1974**, *96*, 998–1003.
[18] F. Wang, L. Liu, W. Wang, S. Li, M. Shi, *Coord. Chem. Rev.* **2012**, *256*, 804–853.
[19] N. Hellou, M. Srebro-Hooper, L. Favereau, F. Zinna, E. Caytan, L. Toupet, V. Dorcet, M. Jean, N. Vanthuyne, J. A. G. Williams, L. Di Bari, J. Autschbach, J. Crassous, *Angew. Chem. Int. Ed.* **2017**, *56*, 8236–8239; *Angew. Chem.* **2017**, *129*, 8348–8351.
[20] J. Yang, K. Li, J. Wang, S. Sun, W. Chi, C. Wang, X. Chang, C. Zou, W. To, M. Li, X. Liu, W. Lu, H. Zhang, C. Che, Y. Chen, *Angew. Chem. Int. Ed.* **2020**, *59*, 6915–6922; *Angew. Chem.* **2020**, *132*, 6982–6989.
[21] R. Tarrieu, I. H. Delgado, F. Zinna, V. Dorcet, S. Colombel-Rouen, C. Crévisy, O. Baslé, J. Bosson, J. Lacour, *Chem. Commun.* **2021**, *57*, 3793–3796.
[22] C.-F. Chen, Y. Shen, in *Helicene Chemistry*, Springer Berlin Heidelberg, Berlin, Heidelberg, **2017**.
[23] K. Dhbaibi, L. Favereau, J. Crassous, *Chem. Rev.* **2019**, *119*, 8846–8953.
[24] E. S. Gauthier, M. Cordier, V. Dorcet, N. Vanthuyne, L. Favereau, J. A. G. Williams, J. Crassous, *Eur. J. Org. Chem.* **2021**, *2021*, 4769–4776.
[25] L. Pallova, L. Abella, M. Jean, N. Vanthuyne, C. Barthes, L. Vendier, J. Autschbach, J. Crassous, S. Bastin, V. César, *Chem. Eur. J.* **2022**, *28*, e202200166.
[26] M. Karras, M. Dąbrowski, R. Pohl, J. Rybáček, J. Vacek, L. Bednárová, K. Grela, I. Starý, I. G. Stará, B. Schmidt, *Chem. Eur. J.* **2018**, *24*, 10994–10998.
[27] I. G. Sánchez, M. Šámal, J. Nejedlý, M. Karras, J. Klívar, J. Rybáček, M. Buděšínský, L. Bednárová, B. Seidlerová, I. G. Stará, I. Starý, *Chem. Commun.* **2017**, *53*, 4370–4373.
[28] N. Hellou, C. Jahier-Diallo, O. Baslé, M. Srebro-Hooper, L. Toupet, T. Roisnel, E. Caytan, C. Roussel, N. Vanthuyne, J. Autschbach, M. Mauduit, J. Crassous, *Chem. Commun.* **2016**, *52*, 9243–9246.
[29] N. Hafedh, L. Favereau, E. Caytan, T. Roisnel, M. Jean, N. Vanthuyne, F. Aloui, J. Crassous, *Chirality* **2019**, *31*, 1005–1013.
[30] A. Macé, N. Hellou, J. Hammoud, C. Martin, E. S. Gauthier, L. Favereau, T. Roisnel, E. Caytan, G. Nasser, N. Vanthuyne, J. A. G. Williams, F. Berrée, B. Carboni, J. Crassous, *Helv. Chim. Acta* **2019**, *102*, e1900044.
[31] E. S. Gauthier, N. Hellou, E. Caytan, S. Del Fré, V. Dorcet, N. Vanthuyne, L. Favereau, M. Srebro-Hooper, J. A. G. Williams, J. Crassous, *Inorg. Chem. Front.* **2021**, *8*, 3916–3925.
[32] E. S. Gauthier, D. Kaczmarczyk, S. Del Fré, L. Favereau, E. Caytan, M. Cordier, N. Vanthuyne, J. A. G. Williams, M. Srebro-Hooper, J. Crassous, *Dalton Trans.* **2022**, *51*, 15571–15578.
[33] E. S. Gauthier, L. Abella, N. Hellou, B. Darquié, E. Caytan, T. Roisnel, N. Vanthuyne, L. Favereau, M. Srebro-Hooper, J. A. G. Williams, J. Autschbach, J. Crassous, *Angew. Chem. Int. Ed.* **2020**, *59*, 8394–8400; *Angew. Chem.* **2020**, *132*, 8472–8478.
[34] N. Saleh, M. Srebro, T. Reynaldo, N. Vanthuyne, L. Toupet, V. Y. Chang, G. Muller, J. A. G. Williams, C. Roussel, J. Autschbach, J. Crassous, *Chem. Commun.* **2015**, *51*, 3754–3757.
[35] H. Isla, N. Saleh, J.-K. Ou-Yang, K. Dhbaibi, M. Jean, M. Dziurka, L. Favereau, N. Vanthuyne, L. Toupet, B. Jamoussi, M. Srebro-Hooper, J. Crassous, *J. Org. Chem.* **2019**, *84*, 5383–5393.
[36] H. Zhang, Q. Cai, D. Ma, *J. Org. Chem.* **2005**, *70*, 5164–5173.
[37] M. S. Newman, D. Lednicer, *J. Am. Chem. Soc.* **1956**, *78*, 4765–4770.
[38] Y. Shen, C.-F. Chen, *Chem. Rev.* **2012**, *112*, 1463–1535.
[39] A. von Zelewsky, in *Stereochemistry of Coordination Compounds*, Wiley, Chichester, England; New York, **1996**.
[40] H. Amouri, M. Gruselle, Chirality, in *Transition Metal Chemistry: Molecules, Supramolecular Assemblies and Materials*, Wiley, Chichester, U.K, **2008**.
[41] M. P. Mitoraj, A. Michalak, T. Ziegler, *J. Chem. Theory Comput.* **2009**, *5*, 962–975.
[42] M. Srebro, A. Michalak, *Inorg. Chem.* **2009**, *48*, 5361–5369.
[43] K. Suzuki, A. Kobayashi, S. Kaneko, K. Takehira, T. Yoshihara, H. Ishida, Y. Siina, S. Oichi, S. Tobita, *Phys. Chem. Chem. Phys.* **2009**, *11*, 9850–9860.
[44] T. Li, D. S. Muthiah Ravinson, R. Haiges, P. I. Djurovich, M. E. Thompson, *J. Am. Chem. Soc.* **2020**, *142*, 6158–6172.
[45] M. Srebro-Hooper, J. Autschbach, *Annu. Rev. Phys. Chem.* **2017**, *68*, 399–420.
[46] J. Autschbach, L. Nitsch-Velasquez, M. Rudolph, *Top. Curr. Chem.* **2011**, *298*, 1–98.
[47] P. A. Summers, A. P. Thomas, T. Kench, J.-B. Vannier, M. K. Kuimova, R. Vilar, *Chem. Sci.* **2021**, *12*, 14624–14634.
[48] T. P. Nicholls, L. K. Burt, P. V. Simpson, M. Massi, A. C. Bissember, *Dalton Trans.* **2019**, *48*, 12749–12754.
[49] Deposition Number(s) 2206259 (for (*P*)-**3**), 2206260 (for (P,C_{Re})-**C**[1]) contain(s) the supplementary crystallographic data for this paper. These data are provided free of charge by the joint Cambridge Crystallographic Data Centre and Fachinformationszentrum Karlsruhe Access Structures service.

Manuscript received: November 8, 2022
Accepted manuscript online: January 16, 2023
Version of record online: March 10, 2023